Environmental Science & Technology

pubs.acs.org/est

Article

New Insights into Unexpected Severe $PM_{2.5}$ Pollution during the SARS and COVID-19 Pandemic Periods in Beijing

Peijie Zuo, Zheng Zong, Bo Zheng, Jianzhou Bi, Qinghua Zhang, Wei Li, Jingwei Zhang, Xuezhi Yang, Zigu Chen, Hang Yang, Dawei Lu,* Qinghua Zhang, Qian Liu, and Guibin Jiang

Cite This: https://doi.org/10.1021/acs.est.1c05383

Read Online

ACCESS | Metrics & More | Article Recommendations | Supporting Information

ABSTRACT: During the SARS period in 2003 and COVID-19 pandemic period in 2020, unexpected severe particulate matter pollution occurred in northern China, although the anthropogenic activities and associated emissions have assumed to be reduced dramatically. This anomalistic increase in $PM_{2.5}$ pollution raises a question about how source emissions impact the air quality during these pandemic periods. In this study, we investigated the stable Cu and Si isotopic compositions and typical source-specific fingerprints of $PM_{2.5}$ and its sources. We show that the primary $PM_{2.5}$ emissions ($PM_{2.5}$ emitted directly from sources) actually had no reduction but redistribution during these pandemic periods, rather than the previous thought of being greatly reduced. This finding provided critical evidence to interpret the anomalistic $PM_{2.5}$ increase during the pandemic periods in north China. Our results also suggested that both the energy structure adjustment and stringent regulations on primary emissions should be synergistically implemented in a regional scale for clean air actions in China.

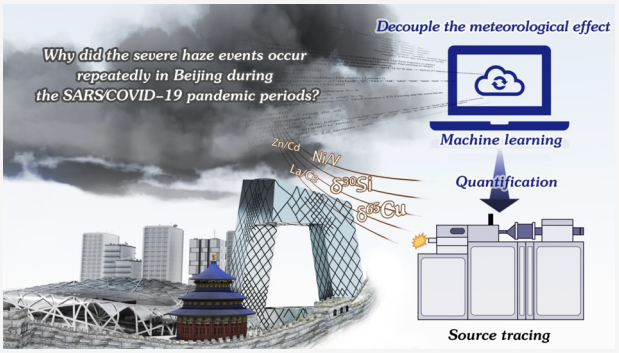

KEYWORDS: *$PM_{2.5}$, SARS, COVID-19, copper isotope, primary emission*

INTRODUCTION

The abrupt outbreak of the corona virus disease 2019 (COVID-19) provides an unprecedented opportunity to estimate the efficiency of interventions in $PM_{2.5}$ emission because the anthropogenic activities and associated primary emissions have been dramatically reduced by social distancing to curb the rapid spread of the virus.[1−5] Many recent studies have quantitatively compared the pollutant levels during the COVID-19 pandemic period with non-pandemic periods, e.g., before or after the pandemic, same period in previous years, and days with similar meteorological conditions.[6−16] Unexpectedly, severe haze events still occurred in northern China (e.g., Beijing) even with strict restriction on human mobility during the COVID-19 pandemic period.[1,17] It was worth noting that the severe $PM_{2.5}$ pollution also occurred in the same region during the SARS pandemic period in 2003, in which human activities have also been extremely decreased.[18] The anomalistic $PM_{2.5}$ pollution not only aggravated the negative public health effect during these pandemic periods[19,20] but also raised the uncertainty about the relationship between the emission and haze pollution.[1,21]

Some studies have interpreted these anomalies in $PM_{2.5}$ level by the enhancement of secondary pollution (secondary aerosols produced by the atmospheric chemical reactions) by assuming that the primary emissions had a well-recognized decline trend during the pandemic periods.[21] Noteworthily, the suppression of human activities mainly reduced the emissions from traffic, but its effects on the residential and power sectors remained unclear. Furthermore, the current studies mainly focused on the observed changes in $PM_{2.5}$ concentrations, with no consideration of the variations in specific fingerprints in $PM_{2.5}$. Thus, the real impacts of emission intervention on the air quality during these pandemic periods were still difficult to be estimated. Particularly, in these cases, the bottom-up emission inventories, which were commonly used to count primary emissions, were hampered by the uncertainties and complex non-linear relationship between $PM_{2.5}$ and primary emissions.[22−25]

Here, we used an alternative method, i.e., top-down observational constraints from high precision source-specific fingerprints, to evaluate the variations in the sources of $PM_{2.5}$ emission during the SARS and COVID-19 pandemic periods. Specifically, the airborne concentrations (ng/m^3) and mass abundance (%) of the primary source markers (including metals, elemental carbon (EC), and soluble ions (K^+, Ca^{2+}, F^-, and

Received: August 10, 2021
Revised: October 27, 2021
Accepted: December 3, 2021

Cl^-)) in $PM_{2.5}$ were investigated to estimate the changes in primary $PM_{2.5}$ emissions. Moreover, stable Cu and distinctive metal elemental ratios were used to quantify the redistribution in the emission intensity of various primary sources during these pandemic periods. In addition, Si isotopic fingerprints combined with bottom-up emission inventories, satellite remote sensing, and backward trajectories analysis were used to assess the robustness of the source apportionment results. The Cu and Si isotopic signatures and distinctive elemental ratios were used due to their special ability in source tracing of particulate matter.[26−28] As a series of clean air policies have been implemented in Beijing from 2003 to 2020, understanding the origins of severe $PM_{2.5}$ pollution during the pandemic periods was crucial for policymaking for future air pollution control.

METHODS

Study Period. Social distancing was implemented from April 20 to June 24, 2003 to curb the spread of SARS pandemic in Beijing, China. Thus, three periods, Pre-SARS period (January 1, 2003 to April 19, 2003), SARS period (April 20, 2003 to June 24, 2003), and After-SARS period (June 25, 2003 to July 24, 2003), were covered to estimate their impact on the primary emission of $PM_{2.5}$. Regarding the COVID-19 pandemic, the first confirmed case was reported in Hubei Province in China in December 2019, and then the first-level public health emergency response (FLPHER) with strict travel restriction measures was triggered throughout China in January 23, 2020. After February 22, 2020, most cities gradually rescinded the FLPHER lockdowns, but there are nonetheless confirmed cases being sporadically reported, making some of the social distancing measures not to be struck down. Therefore, two periods, Pre-COVID-19 period (January 1, 2020 to January 22, 2020) and COVID-19 lockdown period (January 23, 2020, to February 22, 2020), were used to assess the air quality impact of the COVID-19 pandemic. Furthermore, taking account of the potential seasonal variations on the primary $PM_{2.5}$ emissions, the same time period in 2002, 2004, 2018, and 2019 were also used as comparisons.

Sampling of $PM_{2.5}$. The samples of $PM_{2.5}$ and its primary sources (coal burning, soil dust, vehicle emission, biomass burning, and industrial emission) were collected in urban Beijing and Hebei (Supplementary Figure 1). Specifically, ca. 110 m^3/day of air was collected on polypropylene membrane filters (Ø = 90 mm) based on a medium-volume air sampler (Beijing Geological Instrument Co., China) in random days of 2003. For $PM_{2.5}$ samples of 2020, around 130 m^3/day of air was collected onto quartz fiber filters (Ø = 90 mm, MK360, Ahlstrom Munktell, Sweden) by using a middle-volume air sampler (Laoying 2034, Qingdao, China). The sampling site was on a rooftop (~20 m above ground), which was surrounded by a university and several residential buildings. Thus, the sampling site could represent the urban background. The masses of the $PM_{2.5}$ samples were measured by a giant gravimetric balance method.[29] The detailed sampling procedure of primary $PM_{2.5}$ source samples is given in the Supplementary Experimental Section 2.2.

Elemental Analysis. The metal concentrations (Al, Mg, Fe, Zn, Cu, Pb, Ti, Mn, Sr, Nd, Cr, Ni, V, La, Ce, As, Sb, and Cd) of $PM_{2.5}$ and its primary sources were determined by inductively coupled plasma mass spectrometry (ICP-MS, Agilent 8800, USA). The samples were digested with aqua regia (V_{HCl}/V_{HNO3} = 3:1) using a CEM MARS 5 microwave sample preparation system (Matthews, NC, USA) as reported previously.[30] Briefly, 10 mL of aqua regia and 1 mL of 35% (v/v) H_2O_2 were added to the samples; then, the mixture was irradiated at 160 °C for 10 min and 200 °C for 15 min. After cooling, the digests were screened by a 0.22 μm polyether filter and then concentrated to 5 mL at 95 °C. Then, 2 mL of the digests were transferred to a 5 mL polyethylene centrifuge tube and diluted to 4 mL with ultrapure water for ICP-MS analysis. The recoveries of these elements of standard reference materials (NIST-1648a) ranged from 89.7 to 107.2%. The Si concentration measurements of $PM_{2.5}$ and its primary sources were also measured on an Agilent 8800 ICP-MS system. The EC was measured with a DRI thermal/optical carbon analyzer. The soluble ions (K^+, Ca^{2+}, F^-, NO_3^-, SO_4^{2-}, NH_4^+, and Cl^-) in $PM_{2.5}$ were measured with an ion chromatography system (ICS-2000, Dionex Integrion). The detailed pretreatment and analysis procedures are given in the Supplementary Experimental Sections 2.4, 2.7, and 2.9.

Measurement of Cu and Si Isotopic Ratios by MC-ICP-MS. Cu and Si have two stable isotopes (^{63}Cu and ^{65}Cu) and three stable isotopes (^{28}Si, ^{29}Si, and ^{30}Si), respectively. Prior to Cu and Si isotopic analysis, AG MP-1 anion resin-based and Dowex 50WX8 cation resin-based chromatographic methods were used to purify Cu and Si from the digests, respectively.[28,31,32] The detailed Cu and Si purification procedures are given in Supplementary Experimental Sections 2.4 and 2.5. The obtained recoveries of Cu and Si during the sample pretreatment process were ≥94.4%. Then, the Cu and Si isotopic compositions were measured with multicollector inductively coupled plasma mass spectrometry (MC-ICP-MS) (Nu Plasma II, Wrexham, UK) at low-resolution and medium-resolution modes, respectively. The optimized measurement parameters of MC-ICP-MS are given in Supplementary Table 1. The Cu and Si isotopic compositions in samples were reported as δ values ($\delta^{65}Cu$, $\delta^{30}Si$, and $\delta^{29}Si$, in ‰) relative to isotopic standard reference materials (ERM-AE633 for Cu and NIST SRM-8546 for Si) as follows:

$$\delta^{65}\mathrm{Cu} = \left(\frac{(^{65}\mathrm{Cu}/^{63}\mathrm{Cu})_{\mathrm{sample}}}{(^{65}\mathrm{Cu}/^{63}\mathrm{Cu})_{\mathrm{standard}}} - 1 \right) \times 1000‰ \quad (1)$$

$$\delta^{29}\mathrm{Si} = \left(\frac{(^{29}\mathrm{Si}/^{28}\mathrm{Si})_{\mathrm{sample}}}{(^{29}\mathrm{Si}/^{28}\mathrm{Si})_{\mathrm{standard}}} - 1 \right) \times 1000‰ \quad (2)$$

$$\delta^{30}\mathrm{Si} = \left(\frac{(^{30}\mathrm{Si}/^{28}\mathrm{Si})_{\mathrm{sample}}}{(^{30}\mathrm{Si}/^{28}\mathrm{Si})_{\mathrm{standard}}} - 1 \right) \times 1000‰ \quad (3)$$

Here, the mass biases were corrected by a standard-sample-standard bracketing method (SSB).[33] All samples were measured with at least two parallel experiments. The $\delta^{65}Cu$ and $\delta^{30}Si$ values were calibrated based on the mean values of two adjacent standards. Two groups of standard materials, ERM-AE633 and CAG-Cu (an in-house standard), and NIST SRM-8546 and IRMM-017, were used to validate the Cu and Si isotopic measurement methods, respectively. The $\delta^{65}Cu$ and $\delta^{30}Si$ values of CAG-Cu and IRMM-017 solutions were 0.51 ± 0.08 ‰ (mean ± 2SD, n = 40) and −1.38 ± 0.18‰ (mean ± 2SD, n = 36), consistent with the previously reported results,[34,35] which demonstrated that our Cu and Si isotopic analysis methods were accurate and precise.

Bayesian Statistics−Markov Chain Monte Carlo (MCMC) Simulations. To quantitatively estimate the relative proportions of $PM_{2.5}$ from the five emission sources, the

https://doi.org/10.1021/acs.est.1c05383
Environ. Sci. Technol. XXXX, XXX, XXX−XXX

Bayesian model (MixSIAR) with the Markov chain Monte Carlo (MCMC) algorithm was employed.[25] The Bayesian method was a general framework that can determine the probability distribution of source contributions to a mixture and thus has been widely used in source apportionment of air pollutants.[36] The simulation method was based on mass balance of isotope and metal ratios, which can be described according to eq 4 as follows:

$$\begin{pmatrix} \delta^{65}Cu_{PM} \\ (Ni/V)_{PM} \\ (La/Ce)_{PM} \\ \vdots \\ 1 \end{pmatrix} = \begin{pmatrix} \delta^{65}Cu_{coal} & \delta^{65}Cu_{dust} & \cdots & \delta^{65}Cu_{ind.} \\ (Ni/V)_{coal} & (Ni/V)_{dust} & \cdots & (Ni/V)_{ind.} \\ (La/Ce)_{coal} & (La/Ce)_{dust} & & (La/Ce)_{ind.} \\ \vdots & \vdots & \ddots & \vdots \\ 1 & 1 & \cdots & 1 \end{pmatrix} \times \begin{pmatrix} f_{coal} \\ f_{dust} \\ f_{vehicle} \\ f_{bio.} \\ f_{ind.} \end{pmatrix} \quad (4)$$

where PM represents $PM_{2.5}$; f_{coal}, f_{dust}, $f_{vehicle}$, $f_{bio.}$, and $f_{ind.}$ correspond to a fraction of $PM_{2.5}$ emitted from coal burning, dust, vehicle emission, biomass burning, and industrial emission, respectively. The f values reflect the sources' contributions. The detailed procedures of Bayesian model samples are given in the Supplementary Experimental Section 2.12.

RESULTS AND DISCUSSION

Air Quality Trends during the SARS and COVID-19 Pandemic Periods in Beijing. The air quality during different periods of the SARS and COVID-19 pandemics (see Methods) was investigated. Air pollution index (API) values were used to report the air quality in China in 2003, which were provided by the Beijing Environmental Monitoring Center. It was worth noting that the API values were positively correlated with the level of the major air pollutant (see Supplementary Table 2). During the studied periods in 2003, particulate matter was a major air pollutant in most times. As shown in Figure 1a,b, the observed API during the SARS period (April 20 to June 24) in 2003 ranged from 34 to 180, with a mean value of 99.8 ± 34.7 (Supplementary Table 3). These observed levels were close to those in the Pre-SARS period (P = 0.79, Mann−Whitney test), after the SARS period (P = 0.17, Welch's t test) in 2003, and the same periods (April 20 to June 24) in 2002 (P = 0.53, unpaired student t test) and 2004 (P = 0.38, unpaired student t test; Supplementary Table 10). Furthermore, almost half of the days during the SARS period (Supplementary Table 3) showed API values exceeding 100 (equivalent to the observed PM concentrations >150 $\mu g/m^3$). These results indicated that several haze events indeed occurred during the SARS period, which might be driven from complex meteorological transformation and direct emission variations. However, the effect of meteorology failed to be decoupled in 2003 due to the lack of systematic data of meteorological conditions and observed $PM_{2.5}$ concentrations. Thus, an accurate evaluation on the source emission variations is important.

Similarly, several $PM_{2.5}$ pollution events occurred repeatedly in Beijing during the COVID-19 lockdown period, which showed a higher peak observed concentration (207 $\mu g/m^3$) relative to those before the COVID-19 lockdown period (Pre-COVID-19 period) and the same periods in 2018 and 2019 (Figure 1c,d and Supplementary Table 3). We further estimated the above air quality trends by decoupling the effect of meteorology based on an effective deweathering machine learning technique.[37−39] Several days still showed an increase in deweathered $PM_{2.5}$ concentrations during the COVID-19 lockdown periods (Supplementary Figure 2). Specifically, the peak deweathered $PM_{2.5}$ concentrations during the pandemic periods were close to or even higher than those in non-pandemic periods and the same periods in 2018 and 2019 (Supplementary Figure 2). These results appeared to be anomalistic because human mobility and businesses have been dramatically restricted during these pandemic periods. Hence, a sophisticated characterization on the variations in the source emissions is essential for the explanation of air pollution during the SARS and COVID-19 pandemic periods.

Metal Profiles and Cu Isotopic Signatures of Primary $PM_{2.5}$ Sources. To investigate the emission variation during the SARS and COVID-19 pandemic periods, we measured the selected metal element concentrations and Cu isotopic fingerprints of five representative primary sources (coal burning, soil dust, vehicle emission, biomass burning, and industrial emission). The concentrations of most selected metal elements showed a remarkable difference between any two sources (Supplementary Figure 4a and Supplementary Tables 5 and 10). Meanwhile, the concentration ranges of some elements, including Zn, Cu, Pb, Mn, Ni, V, La, As, Sb, and Cd, showed partial overlaps between two or three sectors. Further detailed descriptions on the overlaps are provided in Supplementary discussion in the Supplementary Information. Furthermore, as shown in Supplementary Figure 4b, the ranges of $\delta^{65}Cu$ of $PM_{2.5}$ sources were 0.48−0.72‰ for coal burning (n = 10), −0.17−0.17‰ for dust (n = 20), −0.27−0.05‰ for vehicle emission (n = 6), and −0.95−0.03‰ for biomass burning (n = 10), showing remarkable variations among different sectors. These results were consistent with the previously reported signatures of primary Cu sulfides ($-1‰ < \delta^{65}Cu < 1‰$).[26,40−42] The industrial emission was markedly ^{65}Cu-depleted (−1.92 to −0.66‰, n = 9), which might be attributed to the fact that the Cu in flue gas (emitted by evaporation) tended to enrich the light isotope (^{63}Cu) relative to natural materials in combustion processes.[32] Hence, the Cu isotopic signatures and distinctive metal ratios could indeed record chemical fingerprints of $PM_{2.5}$ in Beijing. More investigations on the isotopic signature of a larger size of source samples and more high-precision tracers (e.g., multiple isotopic signatures) are needed to further improve the accuracy and precision of source apportionment of $PM_{2.5}$ in future studies.

Primary Source Markers and Cu Isotopic Compositions of $PM_{2.5}$. As shown in Figure 2a,b, the EC, soluble ions, and most selected metal elements showed no significant decline (P values > 0.05; Supplementary Table 4) but even an increase in their concentrations and mass abundances in $PM_{2.5}$ (%)

https://doi.org/10.1021/acs.est.1c05383
Environ. Sci. Technol. XXXX, XXX, XXX−XXX

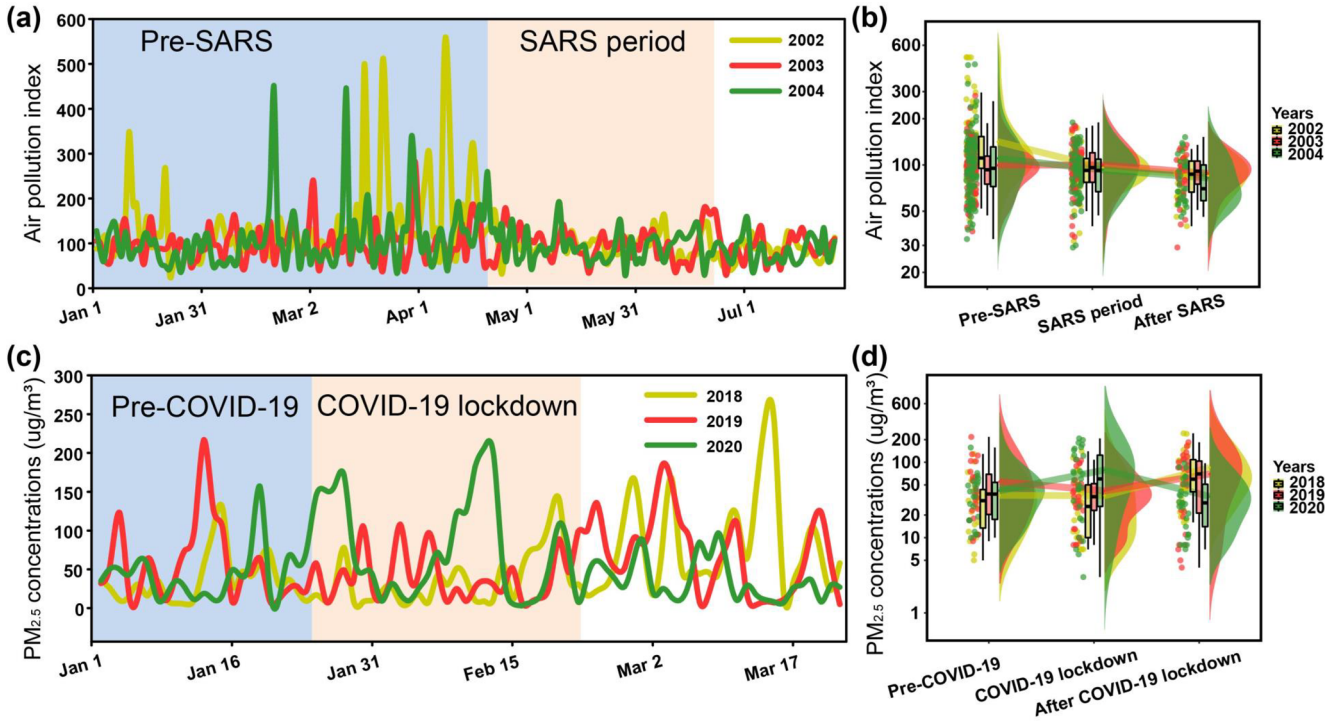

Figure 1. Changes in air quality and $PM_{2.5}$ pollution level before, during, and after the SARS and COVID-19 pandemic periods in Beijing, China. Time series of air quality during the study periods in 2002, 2003, and 2004 (a). Annual variations (2002−2004) of the air quality before, during, and after the SARs pandemic period (b). Time series of $PM_{2.5}$ pollution levels during the study period of 2018−2020 (c). Annual variations (2018−2020) in the distribution of $PM_{2.5}$ concentrations before, during, and after the COVID-19 pandemic period (d). The light blue and light orange areas in panels a and c represent the period before and during the SARS and COVID-19 pandemic, respectively. In panels b and d, each symbol represents an individual subject; statistical analysis (excluded for figure clarity) is fully summarized in Supplementary Table 10. For box plots, the bounds of the box spans from 25 to 75% percentile, the center line represents the median, and the whiskers visualize 5 and 95% of the data points.

during these pandemic periods compared with non-pandemic periods in 2003 and 2020 (Supplementary Figure 5). Their detailed variations in statistical analyses are provided in Supplementary Table 10. The unvaried airborne concentrations and mass abundances of these source-specific markers indicated that the total primary $PM_{2.5}$ emissions might have no substantial reduction in Beijing during these pandemic periods.

We further investigated the metal correlations and Cu isotopic fingerprints of the studied $PM_{2.5}$. The metal correlations could indicate shared sources or similar mechanisms of mobility,[43] and the Cu isotopic composition has been used as a novel marker for source tracing of $PM_{2.5}$ in European cities due to its retainability during anthropogenic or low-temperature environmental processes.[26] As shown in Figure 2c,d,g, in comparison with the non-SARS period (Pre/After SARS period), the correlated metal pairs (e.g., Fe−Mn, Zn−Pb, and La−Ce) showed remarkable decline trends, and the δ^{65}Cu (Cu isotopic composition) distribution range of $PM_{2.5}$ was much wider (P = 0.02, unpaired student's t test) during the SARS period. In 2020, the number of paired correlations between anthropogenic-associated metals (e.g., Pb, Mn, and Cd) showed an increase in $PM_{2.5}$ during the COVID-19 lockdown period against the Pre-COVID-19 period in 2020 (Figure 2e,f). The variations in metal correlations in $PM_{2.5}$ suggested that their source composition might change with some human activities being restricted during the pandemic period. This deduction was consistent with the redistribution of the δ^{65}Cu (Cu isotopic composition) in $PM_{2.5}$ during different periods of SARS and COVID-19 pandemics (Figure 2e,f). It was worth noting that the redistribution in the emission intensity of various sources caused only little impact on the mean pollution levels of most metals in $PM_{2.5}$ during the non-pandemic/pandemic period. Possible explanations for this result were as follows: (i) some sectors might have partial overlaps in some of their elemental compositions, and (ii) the changing effect of one source emission might be overwhelmed by the changes of other emissions in other days.

Tagging $PM_{2.5}$ Metal Fingerprints with Primary Sources. To obtain high-precision estimation on the redistribution in the emission intensity of various sources, we further tagged metal fingerprints (δ^{65}Cu versus Ni/V, La/Ce, Zn/Cd, and Fe/Al ratios) of the $PM_{2.5}$ stratified by pandemic periods with their primary sources. All the eight selected elemental concentrations showed no correlation with Cu during any periods assessed in this study (Figure 2c−f). Despite the four selected metal ratios being well used for source tracing of particulate matter,[44−48] they showed partial overlap in these four metal ratios between sectors in Beijing. For instance, the Ni/V, La/Ce, Zn/Cd, and Fe/Al ratios failed to discern between biomass burning and vehicle emission, soil dust and vehicle emission, vehicle emission and industry, and vehicle emission and biomass burning, respectively (Figure 3). Thus, multiple tracers should be used to identify the redistribution of emission intensity of different sources.

It was worth noting that the metal fingerprint distributions of $PM_{2.5}$ in both pandemic periods were more dispersive than those in the non-pandemic periods, suggesting that the contributing sources tended to be more complex during the pandemic periods. It was interesting that the $PM_{2.5}$ metal fingerprints tended to approach the range of industrial emission during both

https://doi.org/10.1021/acs.est.1c05383
Environ. Sci. Technol. XXXX, XXX, XXX−XXX

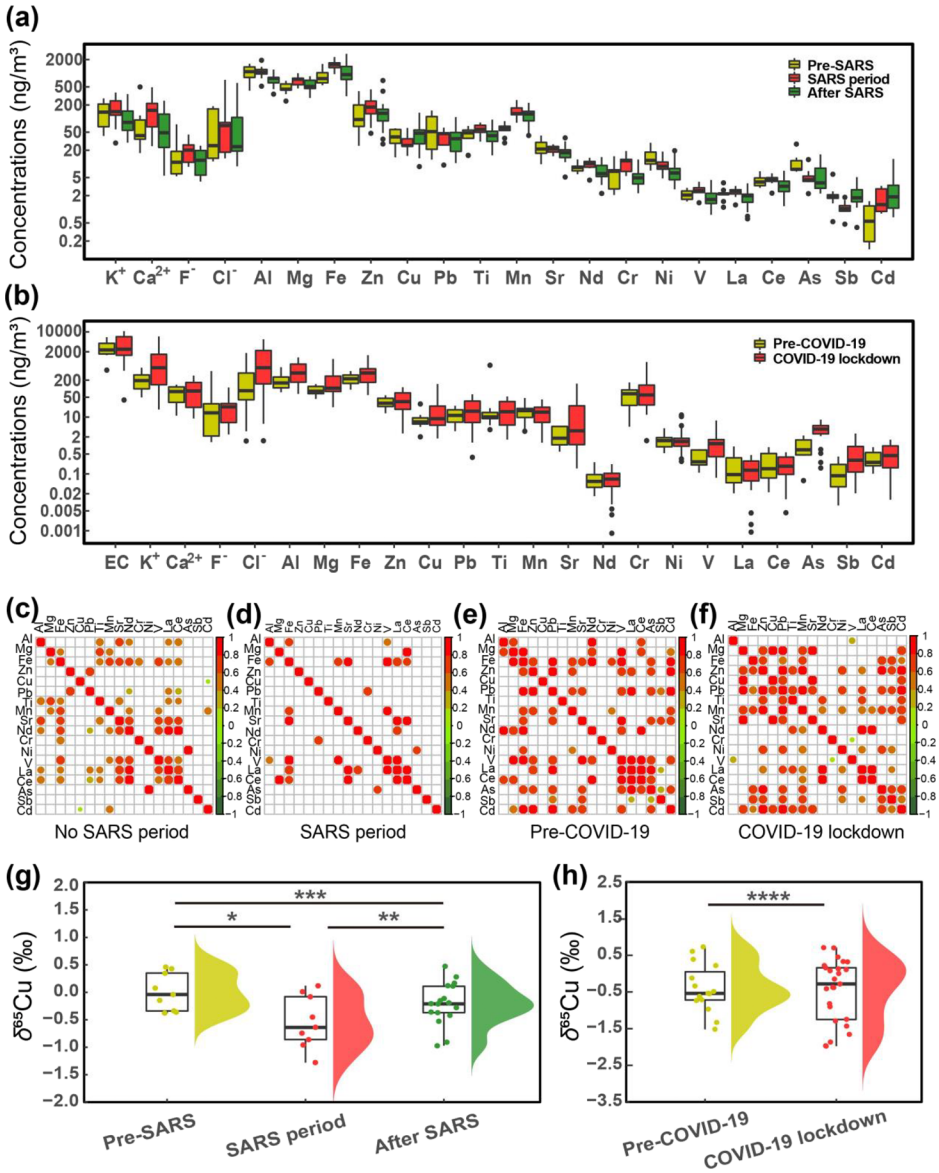

Figure 2. Comparison of pollution characteristics of primary source markers (EC, soluble ions, and metal) and Cu isotopic compositions of $PM_{2.5}$ collected during different periods of SARS and COVID-19 pandemics in Beijing, China. Variations in the concentrations of EC, typical soluble ions, and metal in $PM_{2.5}$ before, during, and after the SARS pandemic periods (a) and before and during COVID-19 pandemic periods (b). Bounds of the box plots span from 25 to 75% percentile, the center line represents the median, and the whiskers visualize 5 and 95% of the data points. Significance was assessed by the unpaired student's *t* test, Welch's *t* test, and Mann−Whitney test, and the statistical results reported in Supplementary Table 10 (data not shown for figure clarity). No measured EC data were hampered by the interference of polypropylene membrane filters of $PM_{2.5}$ samples in 2003. (c−f) Correlation between $PM_{2.5}$ metal concentrations in non-SARS period (Pre/After SARS period) (c), SARS period (d), Pre-COVID-19 period (e), and COVID-19 lockdown period (f). Pearson correlation coefficients (R) are showed by color corresponding to the values given in the left of each figure. All symbols showed here have P values < 0.05, while the blank area means $P > 0.05$. (g, h) Variations in Cu isotopic compositions of $PM_{2.5}$ collected in Beijing during different periods of SARS and COVID-19 pandemics. Each symbol represents an individual subject. SARS: *P_g = 0.02, **P_g = 0.11, and ***P_g = 0.13, unpaired student's *t* test (g). COVID-19: ****P_h = 0.81, unpaired student's *t* test (h). Error bars are excluded for figure clarity, but data are fully reported in Supplementary Table 4.

the SARS and COVID-19 pandemic periods (Figure 3). Considering that the Cu isotopic signature and metal ratios of $PM_{2.5}$ represent a mixed point from different source end-members, these approaches indicated that the contributions of industrial emission might increase. Meanwhile, the Cu level in $PM_{2.5}$ declined in the SARS period, reflecting that the industrial emission enhancement should be along with a reduction in other Cu-enriched sources, e.g., coal burning (Figure 3 and Supplementary Figure 4a). Regarding to the $PM_{2.5}$ levels in the COVID-19 lockdown period, they had a lower Ni/V ratio and an elevated La/Ce ratio relative to those in the Pre-COVID-19 period, which were quite distinct from the vehicle emission range. Thus, we proposed that the contribution from vehicle emission in $PM_{2.5}$ was minimal during the COVID-19 lockdown period. In addition, δ^{65}Cu along with Fe/Al failed to discern industry-associated $PM_{2.5}$ in the COVID-19 lockdown period (Figure 3d), probably due to interferences from the point sources of Al.

Quantification of the Primary Source Contributions. To quantitatively assess the redistribution in the emission

https://doi.org/10.1021/acs.est.1c05383
Environ. Sci. Technol. XXXX, XXX, XXX−XXX

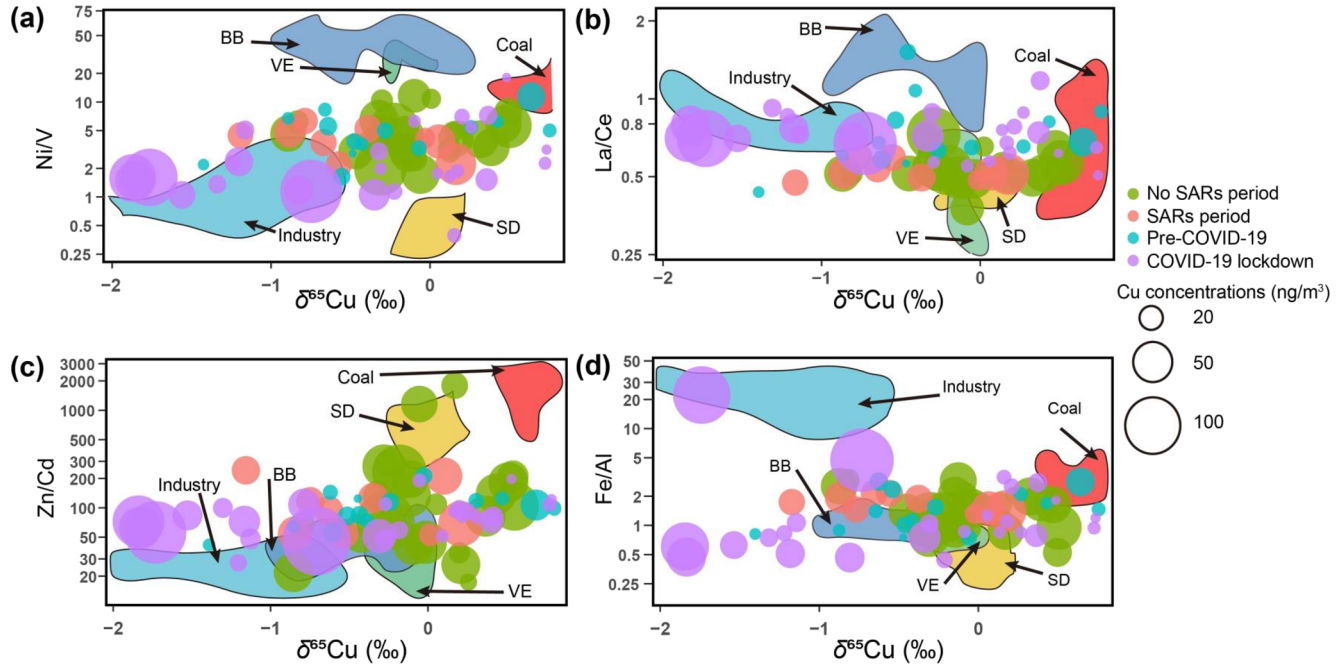

Figure 3. Cu isotopic compositions versus Ni/V (a), La/Ce (b), Zn/Cd (c), and Fe/Al (d) ratios of $PM_{2.5}$ and primary sources in Beijing during different periods of SARS and COVID-19 pandemics. Symbol sizes of circles correspond to concentrations of Cu in $PM_{2.5}$. The terms Coal, SD, VE, BB, and Industry in (a–d) represent coal burning emission (n = 10), soil dust (n = 20), vehicle emission (n = 6), biomass burning emission (n = 10), and industrial emission (n = 9), respectively.

intensity of various sources, we conducted a mass balance calculation based on the selected metal fingerprints (the measured Cu isotopic signatures and selected elemental ratios except Fe/Al) of $PM_{2.5}$ and its sources (five potential sources reported in previous studies[49]) using the Bayesian–Markov chain Monte Carlo (MCMC) simulation method.[25] We estimated that the contributions of coal burning, dust, vehicle emission, and biomass burning decreased from 22.1 ± 13.4, 41.3 ± 16.5, 7.3 ± 6.2, and 4.4 ± 4.1% in the Pre-SARS period to 9.1 ± 6.7, 33.2 ± 18.8, 3.3 ± 3.1, and 2.2 ± 2.1% in the SARS period in 2003, while the contribution of industrial emission increased from 24.8 ± 12.0 to 52.1 ± 17.5% (Figure 4a). After the SARS-associated social distancing was rescinded on June 24, 2003, the contribution from industrial emission decreased back to 24.6 ± 15.4% (Figure 4a). More source end-members are needed to provide more accurate source apportionment in future studies.

To verify the source apportionment results, we also used Si isotopic fingerprints, another tool for source tracing of $PM_{2.5}$,[28] to evaluate the redistribution in the emission intensity of various sources. Specifically, we calculated the Si isotopic compositions of $PM_{2.5}$ based on the Si isotopic signatures of primary sources and their aforementioned relative contributions, and compared them with the observed values. The calculation processes are provided in Supplementary Experimental Section 2.6. As shown in Supplementary Figure 6, the calculated Si isotopic compositions of $PM_{2.5}$ in different periods of the SARS pandemic were consistent with the observed values. The largest net difference between the calculated values and observed data was 0.22‰, which was smaller than the method uncertainty (0.28‰). These supported the robustness of the aforementioned source apportionment results.

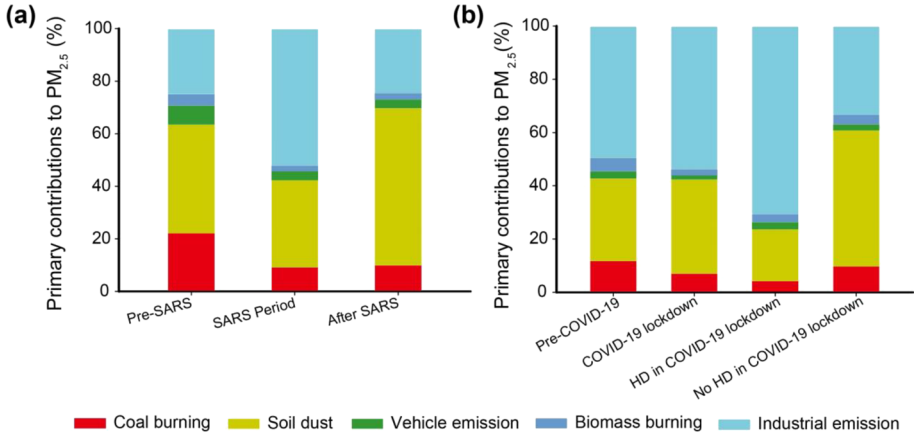

Figure 4. Variations in the relative contributions of individual primary sources to $PM_{2.5}$ during different periods of SARS (a) and COVID-19 pandemics (b). The change of primary source contributions to haze days (HD) and no-haze days (No HD) during COVID-lockdown periods. Haze days indicate the $PM_{2.5}$ pollution levels >100 $\mu g/m^3$. The uncertainties for these results are given in Supplementary Table 6.

https://doi.org/10.1021/acs.est.1c05383
Environ. Sci. Technol. XXXX, XXX, XXX–XXX

During the COVID-19 lockdown period, the average contribution of industrial emission had a small enhancement (~4.4%), while the other sectors showed decline trends compared with the Pre-COVID-19 period (Figure 4b and Supplementary Table 6). For example, the industrial emission contribution decreased from 49.4 ± 11.7% (Pre-COVID-19 period) to 33.2 ± 11.8% in no-haze days ($PM_{2.5}$ < 100 $\mu g/m^3$) during the COVID-19 lockdown period (Figure 4b and Supplementary Table 6). This decline trend was consistent with the reduction of industrial activities predicted by the updated monthly emission inventories (a multi-resolution emission inventory model for China (MEIC)[23]) in 2020 (see Supplementary Table 7). While in haze days ($PM_{2.5}$ > 100 $\mu g/m^3$) during the COVID-19 lockdown period (January 25 to 28 and February 9 to 13), the contribution of industrial emission increased sharply to 70.6 ± 10.4% (Figure 4b).

We further investigated the industrial hot-value areas' count number in Beijing-Tianjin-Hebei regions in these haze event days based on Moderate-resolution Imaging Spectroradiometer (MODIS). The hot-value industrial production (e.g., steel and power plants) showed a significant increase in this region relative to the same period in 2019 (Supplementary Figure 7).[50,51] For instance, from January 23 to February 13 in 2020, the number of industrial high thermal value zones in major cities in the North China Plain had reached 848, increasing by 22.4% relative to the same term in 2019.[50] Furthermore, the production of pig iron and crude steel in China in January and February in 2020 (partially overlap with the COVID-19 lockdown period) was 132.34 million tons and 154.7 million tons, respectively, both increasing by 3.1% relative to the same term in 2019. The social stock of five kinds of steel (rebar, wire, hot rolled coil, cold rolled coil, and medium plate) in the major cities in China was 8.12 million tons at the end of January and increase to 19.05 million tons at the end of February in 2020.[51] That is, the PM-associated industrial emissions actually increased, although the level of overall industrial activities decreased in the COVID-19 lockdown period.

Furthermore, backward trajectory analysis revealed that the transport of air mass to Beijing during the two assessed haze events was confined to <0.5 km, linked to the compressed boundary layer (Supplementary Figure 8).[52] These meteorological characteristics supported the inputs of the elevated upwind regional $PM_{2.5}$ emissions from, for example, hot-value industrial regions, to Beijing. It was worth noting that the metal fingerprints of these sources were similar between Beijing and Hebei (P values > 0.05, Supplementary Figure 9), and hence the aforementioned source apportionment results did not discriminate the contribution of Beijing and Hebei. A more accurate estimate of the inter-regional transport of $PM_{2.5}$ between Beijing and Hebei may be quantified using a chemical transport model in future studies.[53]

Environmental Implications. This study demonstrated the feasibility of a combination of a stable isotopic signature and distinctive metal ratios (valuable tracers in other regions) in source tracing of $PM_{2.5}$, and also proposed a practical source apportionment method by coupling the δ^{65}Cu-based quantification with δ^{30}Si-based robustness assessment. The self-verifiable methodology developed herein could be applicable to explain other PM pollution events in other countries/regions. Moreover, our comprehensive analyses of the primary source-specific markers, δ^{65}Cu and δ^{30}Si, provided scientific evidence that the primary $PM_{2.5}$ emission in Beijing did not decline as expected but dramatically redistributed during the SARS and COVID-19 pandemic periods. Specifically, the emission reductions from coal burning, vehicle emission, and biomass burning were almost compensated by the enhancement of industrial emissions, e.g., steel and power plants in the upwind regions of Beijing. Additionally, as recently reported, secondary aerosol formation processes were also enhanced dramatically during the pandemic periods due probably to the rapid changes in meteorological conditions or significant increase in atmospheric oxidative capacity.[21,37] During the COVID-19 lockdown in Beijing, the secondary particles (secondary inorganic/organic aerosols) contributed to roughly half of $PM_{2.5}$ mass (Supplementary Table 4 and Supplementary Figure 10). Therefore, due to less reduction but even an enhancement in primary emission and secondary $PM_{2.5}$ formation,[21] unexpected air pollution events ultimately occurred during these pandemic periods in Beijing.

In addition, the anomalistic $PM_{2.5}$ pollution during the pandemic periods raised some doubt among the Chinese public and policymakers as to whether the exact sources have been identified or controlled, making the current prioritization of clean air actions to be ambiguous. In this study, the metal fingerprints of $PM_{2.5}$ during the pandemic periods remained to be covered by the ranges of source fingerprints, suggesting that these sectors remained to be exact sources of $PM_{2.5}$ during these pandemic periods. Therefore, this study provides scientific indication that the existing emission regulations on these source sectors were still effective, while the regulation intensity should be adjusted with the redistribution of the emission intensity of various sources. Furthermore, this study could provide important information for studying the mechanisms of these episodic haze events. Because most related studies with atmospheric chemistry and transport simulations assumed the primary emissions to be declined at different levels, these results obtained by novel techniques could provide data for emission settings in the models, e.g., the Weather Research and Forecast model online coupled with full gaseous and aerosol chemistry (WRF-Chem).

The disentanglement of the anomalistic $PM_{2.5}$ pollution during these pandemic periods can also provide an important reference for future air pollution control. In the clean air actions in the past decade (from 2003 to 2020), small and polluting factories and outdated industrial capacities had been phased out from Beijing, and the industrial emission standards had also been strengthened.[53] However, the severe $PM_{2.5}$ pollution during the COVID-19 lockdown period remained to be dominant by industrial emissions, particularly steel and power plants in upwind regions of Beijing (e.g., Hebei, Shandong). Therefore, a joint action with energy structure adjustment in a regional scale (e.g., Beijing-Tianjin-Hebei) should still be of high priority for making future clean air policies. Furthermore, no remarkable decline in primary $PM_{2.5}$ emissions were found in Beijing during the pandemic periods, indicating that the public health associated social distancing measures could not replace the regulations on air pollutant emissions. Particularly, the current energy structure has not been fully optimized, and thereby independent and stringent regulations on $PM_{2.5}$ emissions should be constantly implemented to ensure the air quality in China.

■ ASSOCIATED CONTENT

Supporting Information

The Supporting Information is available free of charge at https://pubs.acs.org/doi/10.1021/acs.est.1c05383.

https://doi.org/10.1021/acs.est.1c05383
Environ. Sci. Technol. XXXX, XXX, XXX−XXX

Additional discussion on the metal profile of $PM_{2.5}$ and primary sources; additional experimental details, materials, and methods, including sampling, machine learning application, and the Bayesian model; additional figures of deweathered $PM_{2.5}$ concentrations, mass abundance of primary markers, and metal fingerprints of sources (PDF)

Supplementary Tables, e.g., instrument parameters, raw data of figures, statistical analysis results (XLSX)

AUTHOR INFORMATION

Corresponding Author

Dawei Lu − *State Key Laboratory of Environmental Chemistry and Ecotoxicology, Research Center for Eco-Environmental Sciences, Chinese Academy of Sciences, Beijing 100085, China; University of Chinese Academy of Sciences, Beijing 100190, China;* orcid.org/0000-0002-8128-6367; Email: dwlu@rcees.ac.cn

Authors

Peijie Zuo − *State Key Laboratory of Environmental Chemistry and Ecotoxicology, Research Center for Eco-Environmental Sciences, Chinese Academy of Sciences, Beijing 100085, China; University of Chinese Academy of Sciences, Beijing 100190, China*

Zheng Zong − *CAS Key Laboratory of Coastal Environmental Processes and Ecological Remediation, Yantai Institute of Coastal Zone Research, Chinese Academy of Sciences, Yantai, Shandong 264003, China;* orcid.org/0000-0002-3666-6539

Bo Zheng − *Institute of Environment and Ecology, Tsinghua Shenzhen International Graduate School, Tsinghua University, Shenzhen 5518055, China*

Jianzhou Bi − *University of Chinese Academy of Sciences, Beijing 100190, China*

Qinghua Zhang − *State Key Laboratory of Environmental Chemistry and Ecotoxicology, Research Center for Eco-Environmental Sciences, Chinese Academy of Sciences, Beijing 100085, China*

Wei Li − *Biomedical Engineering Institute, School of Control Science and Engineering, Shandong University, Jinan 250061, China*

Jingwei Zhang − *State Key Laboratory of Atmospheric Boundary Layer Physics and Atmospheric Chemistry, Institute of Atmospheric Physics, Chinese Academy of Sciences, Beijing 100029, China*

Xuezhi Yang − *State Key Laboratory of Environmental Chemistry and Ecotoxicology, Research Center for Eco-Environmental Sciences, Chinese Academy of Sciences, Beijing 100085, China*

Zigu Chen − *State Key Laboratory of Environmental Chemistry and Ecotoxicology, Research Center for Eco-Environmental Sciences, Chinese Academy of Sciences, Beijing 100085, China; University of Chinese Academy of Sciences, Beijing 100190, China*

Hang Yang − *State Key Laboratory of Environmental Chemistry and Ecotoxicology, Research Center for Eco-Environmental Sciences, Chinese Academy of Sciences, Beijing 100085, China; University of Chinese Academy of Sciences, Beijing 100190, China*

Qinghua Zhang − *State Key Laboratory of Environmental Chemistry and Ecotoxicology, Research Center for Eco-Environmental Sciences, Chinese Academy of Sciences, Beijing 100085, China; University of Chinese Academy of Sciences, Beijing 100190, China*

Qian Liu − *State Key Laboratory of Environmental Chemistry and Ecotoxicology, Research Center for Eco-Environmental Sciences, Chinese Academy of Sciences, Beijing 100085, China; University of Chinese Academy of Sciences, Beijing 100190, China;* orcid.org/0000-0001-8525-7961

Guibin Jiang − *State Key Laboratory of Environmental Chemistry and Ecotoxicology, Research Center for Eco-Environmental Sciences, Chinese Academy of Sciences, Beijing 100085, China; University of Chinese Academy of Sciences, Beijing 100190, China;* orcid.org/0000-0002-6335-3917

Complete contact information is available at: https://pubs.acs.org/10.1021/acs.est.1c05383

Author Contributions

D.L. conceived and designed the research; Q.L., and G.J. supervised this project; D.L. and P.Z. performed most of the measurements and data analyses; Z.Z., B.Z., W.L., J.Z., and J.B. helped developed the mathematical models and emission inventories; Q.Z., X.Y., Z.C., and H.Y. participated in the discussion; Q.Z. provided the samples; D.L., P.Z., and Q.L. wrote the paper.

Notes

The authors declare no competing financial interest.

ACKNOWLEDGMENTS

This work was financially supported by the National Natural Science Foundation of China (nos. 21904134, 22188102, 91743206, 21825403, 22193051, and 92143301), the Chinese Academy of Sciences (nos. XDPB2003, ZDBS-LY-DQC030), and the Sanming Project of Medicine in Shenzhen (no. SZSM201811070). We thank Dr. Chenglong Zhang, Pengfei Liu, Chaoyang Xue, Zhuobiao Ma, and Huan Zhang and Mr. Zhixiang Ma, Xiangwei Meng, and Haiyan Ran for help with sample collection.

REFERENCES

(1) Le, T.; Wang, Y.; Liu, L.; Yang, J.; Yung, Y. L.; Li, G.; Seinfeld, J. H. Unexpected air pollution with marked emission reductions during the COVID-19 outbreak in China. *Science* **2020**, *369*, 702−706.

(2) He, G.; Pan, Y.; Tanaka, T. The short-term impacts of COVID-19 lockdown on urban air pollution in China. *Nat. Sustain.* **2020**, 1005.

(3) Cohen, J.; Kupferschmidt, K. Strategies shift as coronavirus pandemic looms. *Science* **2020**, *367*, 962−963.

(4) Lelieveld, J.; Evans, J. S.; Fnais, M.; Giannadaki, D.; Pozzer, A. The contribution of outdoor air pollution sources to premature mortality on a global scale. *Nature* **2015**, *525*, 367−371.

(5) Miyazaki, K.; Bowman, K.; Sekiya, T.; Takigawa, M.; Neu, J. L.; Sudo, K.; Osterman, G.; Eskes, H. Global tropospheric ozone responses to reduced NO_X emissions linked to the COVID-19 worldwide lockdowns. *Sci. Adv.* **2021**, *7*, No. eabf7460.

(6) Sharma, S.; Zhang, M. Y.; Anshika; Gao, J. S.; Zhang, H. L.; Kota, S. H. Effect of restricted emissions during COVID-19 on air quality in India. *Sci. Total Environ.* **2020**, *728*, 8.

(7) Tobías, A.; Carnerero, C.; Reche, C.; Massagué, J.; Via, M.; Minguillón, M. C.; Alastuey, A.; Querol, X. Changes in air quality during the lockdown in Barcelona (Spain) one month into the SARS-CoV-2 epidemic. *Sci. Total Environ.* **2020**, *726*, 138540.

(8) Yang, Y.; Ren, L.; Li, H.; Wang, H.; Wang, P.; Chen, L.; Yue, X.; Liao, H. Fast Climate Responses to Aerosol Emission Reductions During the COVID-19 Pandemic. *Geophys. Res. Lett.* **2020**, *47*, No. e2020GL089788.

(9) Dai, Q.; Liu, B.; Bi, X.; Wu, J.; Liang, D.; Zhang, Y.; Feng, Y.; Hopke, P. K. Dispersion Normalized PMF Provides Insights into the Significant Changes in Source Contributions to $PM_{2.5}$ after the COVID-19 Outbreak. *Environ. Sci. Technol.* **2020**, *54*, 9917−9927.
(10) Sun, Y.; Lei, L.; Zhou, W.; Chen, C.; He, Y.; Sun, J.; Li, Z.; Xu, W.; Wang, Q.; Ji, D.; Fu, P.; Wang, Z.; Worsnop, D. R. A chemical cocktail during the COVID-19 outbreak in Beijing, China: Insights from six-year aerosol particle composition measurements during the Chinese New Year holiday. *Sci. Total Environ.* **2020**, *742*, 140739.
(11) Lian, X.; Huang, J.; Huang, R.; Liu, C.; Wang, L.; Zhang, T. Impact of city lockdown on the air quality of COVID-19-hit of Wuhan city. *Sci. Total Environ.* **2020**, *742*, 140556.
(12) Wang, Y.; Wen, Y.; Wang, Y.; Zhang, S.; Zhang, K. M.; Zheng, H.; Xing, J.; Wu, Y.; Hao, J. Four-Month Changes in Air Quality during and after the COVID-19 Lockdown in Six Megacities in China. *Environ. Sci. Technol. Lett.* **2020**, *7*, 802−808.
(13) Yin, Z.; Zhang, Y.; Wang, H.; Li, Y. Evident PM2.5 Drops in the East of China due to the COVID-19 Quarantines in February. *Atmos. Chem. Phys. Discuss.* **2020**, *2020*, 1−18.
(14) Kim, H. C.; Kim, S.; Cohen, M.; Bae, C.; Lee, D.; Saylor, R.; Bae, M.; Kim, E.; Kim, B. U.; Yoon, J. H.; Stein, A. Quantitative assessment of changes in surface particulate matter concentrations over China during the COVID-19 pandemic and their implications for Chinese economic activity. *Atmos. Chem. Phys.* **2020**, *2020*, 1−21.
(15) Yang, J.; Wen, Y.; Wang, Y.; Zhang, S.; Pinto, J. P.; Pennington, E. A.; Wang, Z.; Wu, Y.; Sander, S. P.; Jiang, J. H.; Hao, J.; Yung, Y. L.; Seinfeld, J. H. From COVID-19 to future electrification: Assessing traffic impacts on air quality by a machine-learning model. *Proc. Natl. Acad. Sci. U. S. A.* **2021**, *118*, No. e2102705118.
(16) Venter, Z. S.; Aunan, K.; Chowdhury, S.; Lelieveld, J. COVID-19 lockdowns cause global air pollution declines. *Proc. Natl. Acad. Sci. U. S. A.* **2020**, *117*, 18984−18990.
(17) Lu, D.; Zhang, J.; Xue, C.; Zuo, P.; Chen, Z.; Zhang, L.; Ling, W.; Liu, Q.; Jiang, G. COVID-19-Induced Lockdowns Indicate the Short-Term Control Effect of Air Pollutant Emission in 174 Cities in China. *Environ. Sci. Technol.* **2021**, *55*, 4094−4102.
(18) Lang, J.; Zhang, Y.; Zhou, Y.; Cheng, S.; Chen, D.; Guo, X.; Chen, S.; Li, X.; Xing, X.; Wang, H. Trends of PM2.5 and Chemical Composition in Beijing, 2000-2015. *Aerosol Air Qual. Res.* **2017**, *17*, 412−425.
(19) Wu, X.; Nethery, R. C.; Sabath, M. B.; Braun, D.; Dominici, F. Air pollution and COVID-19 mortality in the United States: Strengths and limitations of an ecological regression analysis. *Sci. Adv.* **2020**, *6*, No. eabd4049.
(20) Chen, K.; Wang, M.; Huang, C.; Kinney, P. L.; Anastas, P. T. Air pollution reduction and mortality benefit during the COVID-19 outbreak in China. *Lancet Planet. Health* **2020**, *4*, e210−e212.
(21) Huang, X.; Ding, A.; Gao, J.; Zheng, B.; Zhou, D.; Qi, X.; Tang, R.; Wang, J.; Ren, C.; Nie, W.; Chi, X.; Xu, Z.; Chen, L.; Li, Y.; Che, F.; Pang, N.; Wang, H.; Tong, D.; Qin, W.; Cheng, W.; Liu, W.; Fu, Q.; Liu, B.; Chai, F.; Davis, S. J.; Zhang, Q.; He, K. Enhanced secondary pollution offset reduction of primary emissions during COVID-19 lockdown in China. *Natl. Sci. Rev.* **2021**, nwaa137.
(22) Xing, J.; Li, S.; Jiang, Y.; Wang, S.; Ding, D.; Dong, Z.; Zhu, Y.; Hao, J. Quantifying the emission changes and associated air quality impacts during the COVID-19 pandemic in North China Plain: a response modeling study. *Atmos. Chem. Phys. Discuss.* **2020**, *2020*, 1−28.
(23) Zheng, B.; Zhang, Q.; Geng, G.; Chen, C.; Shi, Q.; Cui, M.; Lei, Y.; He, K. Changes in China's anthropogenic emissions and air quality during the COVID-19 pandemic in 2020. *Earth Syst. Sci. Data* **2021**, *13*, 2895−2907.
(24) Lv, Z.; Wang, X.; Deng, F.; Ying, Q.; Archibald, A. T.; Jones, R. L.; Ding, Y.; Cheng, Y.; Fu, M.; Liu, Y.; Man, H.; Xue, Z.; He, K.; Hao, J.; Liu, H. Source-Receptor Relationship Revealed by the Halted Traffic and Aggravated Haze in Beijing during the COVID-19 Lockdown. *Environ. Sci. Technol.* **2020**, *54*, 15660−15670.
(25) Bikkina, S.; Andersson, A.; Kirillova, E. N.; Holmstrand, H.; Tiwari, S.; Srivastava, A. K.; Bisht, D. S.; Gustafsson, Ö. Air quality in megacity Delhi affected by countryside biomass burning. *Nat. Sustain.* **2019**, *2*, 200−205.
(26) Gonzalez, R. O.; Strekopytov, S.; Amato, F.; Querol, X.; Reche, C.; Weiss, D. New Insights from Zinc and Copper Isotopic Compositions into the Sources of Atmospheric Particulate Matter from Two Major European Cities. *Environ. Sci. Technol.* **2016**, *50*, 9816−9824.
(27) Huang, Q.; Chen, J.; Huang, W.; Fu, P.; Guinot, B.; Feng, X.; Shang, L.; Wang, Z.; Wang, Z.; Yuan, S.; Cai, H.; Wei, L.; Yu, B. Isotopic composition for source identification of mercury in atmospheric fine particles. *Atmos. Chem. Phys.* **2016**, *16*, 11773−11786.
(28) Lu, D.; Liu, Q.; Yu, M.; Yang, X.; Fu, Q.; Zhang, X.; Mu, Y.; Jiang, G. Natural Silicon Isotopic Signatures Reveal the Sources of Airborne Fine Particulate Matter. *Environ. Sci. Technol.* **2018**, *52*, 1088−1095.
(29) Wang, Y.; Yang, W.; Han, B.; Zhang, W.; Chen, M.; Bai, Z. Gravimetric analysis for PM2.5 mass concentration based on year-round monitoring at an urban site in Beijing. *J. Environ. Sci.* **2016**, *40*, 154−160.
(30) Zhang, L.; Jin, X.; Johnson, A. C.; Giesy, J. P. Hazard posed by metals and As in PM2.5 in air of five megacities in the Beijing-Tianjin-Hebei region of China during APEC. *Environ. Sci. Pollut. Res.* **2016**, *23*, 17603−17612.
(31) Van Heghe, L.; Engström, E.; Rodushkin, I.; Cloquet, C.; Vanhaecke, F. Isotopic analysis of the metabolically relevant transition metals Cu, Fe and Zn in human blood from vegetarians and omnivores using multi-collector ICP-mass spectrometry. *J. Anal. At. Spectrom.* **2012**, *27*, 1327.
(32) Lu, D.; Zhang, T.; Yang, X.; Su, P.; Liu, Q.; Jiang, G. Recent advances in the analysis of non-traditional stable isotopes by multi-collector inductively coupled plasma mass spectrometry. *J. Anal. At. Spectrom.* **2017**, *32*, 1848−1861.
(33) Lu, D.; Liu, Q.; Zhang, T.; Cai, Y.; Yin, Y.; Jiang, G. Stable silver isotope fractionation in the natural transformation process of silver nanoparticles. *Nat. Nanotechnol.* **2016**, *11*, 682−686.
(34) Li, J.; Tang, S.-h.; Zhu, X.-k.; Li, Z.-h.; Li, S.-Z.; Yan, B.; Wang, Y.; Sun, J.; Shi, Y.; Dong, A.; Belshaw, N. S.; Zhang, X.; Liu, S.-a.; Liu, J.-h.; Wang, D.; Jiang, S.-y.; Hou, K.; Cohen, A. S. Basaltic and Solution Reference Materials for Iron, Copper and Zinc Isotope Measurements. *Geostand. Geoanal. Res.* **2019**, *43*, 163−175.
(35) Zambardi, T.; Poitrasson, F. Precise Determination of Silicon Isotopes in Silicate Rock Reference Materials by MC-ICP-MS. *Geostand. Geoanal. Res.* **2011**, *35*, 89−99.
(36) Zong, Z.; Wang, X.; Tian, C.; Chen, Y.; Fang, Y.; Zhang, F.; Li, C.; Sun, J.; Li, J.; Zhang, G. First Assessment of NO_x Sources at a Regional Background Site in North China Using Isotopic Analysis Linked with Modeling. *Environ. Sci. Technol.* **2017**, *51*, 5923−5931.
(37) Shi, Z.; Song, C.; Liu, B.; Lu, G.; Xu, J.; Van Vu, T.; Elliott, R. J. R.; Li, W.; Bloss, W. J.; Harrison, R. M. Abrupt but smaller than expected changes in surface air quality attributable to COVID-19 lockdowns. *Sci. Adv.* **2021**, *7*, No. eabd6696.
(38) Grange, S. K.; Carslaw, D. C.; Lewis, A. C.; Boleti, E.; Hueglin, C. Random forest meteorological normalisation models for Swiss PM_{10} trend analysis. *Atmos. Chem. Phys.* **2018**, *18*, 6223−6239.
(39) Vu, T. V.; Shi, Z.; Cheng, J.; Zhang, Q.; He, K.; Wang, S.; Harrison, R. M. Assessing the impact of clean air action on air quality trends in Beijing using a machine learning technique. *Atmos. Chem. Phys.* **2019**, *19*, 11303−11314.
(40) Kimball, B. E.; Mathur, R.; Dohnalkova, A. C.; Wall, A. J.; Runkel, R. L.; Brantley, S. L. Copper isotope fractionation in acid mine drainage. *Geochim. Cosmochim. Acta* **2009**, *73*, 1247−1263.
(41) Dong, S.; Weiss, D. J.; Strekopytov, S.; Kreissig, K.; Sun, Y.; Baker, A. R.; Formenti, P. Stable isotope ratio measurements of Cu and Zn in mineral dust (bulk and size fractions) from the Taklimakan Desert and the Sahel and in aerosols from the eastern tropical North Atlantic Ocean. *Talanta* **2013**, *114*, 103−109.
(42) Little, S. H.; Vance, D.; Walker-Brown, C.; Landing, W. M. The oceanic mass balance of copper and zinc isotopes, investigated by analysis of their inputs, and outputs to ferromanganese oxide sediments. *Geochim. Cosmochim. Acta* **2014**, *125*, 673−693.

https://doi.org/10.1021/acs.est.1c05383
Environ. Sci. Technol. XXXX, XXX, XXX−XXX

(43) Gunawardana, C.; Egodawatta, P.; Goonetilleke, A. Adsorption and mobility of metals in build-up on road surfaces. *Chemosphere* **2015**, *119*, 1391−1398.
(44) Chiffllet, S.; Amouroux, D.; Bérail, S.; Barre, J.; Van, T. C.; Baltrons, O.; Brune, J.; Dufour, A.; Guinot, B.; Mari, X. Origins and discrimination between local and regional atmospheric pollution in Haiphong (Vietnam), based on metal(loid) concentrations and lead isotopic ratios in PM10. *Environ. Sci. Pollut. Res.* **2018**, *25*, 26653−26668.
(45) Bozlaker, A.; Prospero, J. M.; Fraser, M. P.; Chellam, S. Quantifying the contribution of long-range Saharan dust transport on particulate matter concentrations in Houston, Texas, using detailed elemental analysis. *Environ. Sci. Technol.* **2013**, *47*, 10179−10187.
(46) Arditsoglou, A.; Samara, C. Levels of total suspended particulate matter and major trace elements in Kosovo: a source identification and apportionment study. *Chemosphere* **2005**, *59*, 669−678.
(47) Moreno, T.; Querol, X.; Alastuey, A.; Pey, J.; Minguillón, M. C.; Pérez, N.; Bernabé, R. M.; Blanco, S.; Cárdenas, B.; Gibbons, W. Lanthanoid geochemistry of urban atmospheric particulate matter. *Environ. Sci. Technol.* **2008**, *42*, 6502−6507.
(48) Kulkarni, P.; Chellam, S.; Fraser, M. P. Tracking Petroleum Refinery Emission Events Using Lanthanum and Lanthanides as Elemental Markers for PM2.5. *Environ. Sci. Technol.* **2007**, *41*, 6748−6754.
(49) Huang, R. J.; Zhang, Y.; Bozzetti, C.; Ho, K. F.; Cao, J. J.; Han, Y.; Daellenbach, K. R.; Slowik, J. G.; Platt, S. M.; Canonaco, F.; Zotter, P.; Wolf, R.; Pieber, S. M.; Bruns, E. A.; Crippa, M.; Ciarelli, G.; Piazzalunga, A.; Schwikowski, M.; Abbaszade, G.; Schnelle-Kreis, J.; Zimmermann, R.; An, Z.; Szidat, S.; Baltensperger, U.; El Haddad, I.; Prevot, A. S. High secondary aerosol contribution to particulate pollution during haze events in China. *Nature* **2014**, *514*, 218−222.
(50) *Ministry of Ecology and Environment of the People's Republic of China*. http://www.mee.gov.cn/ywgz/dqhjbh/dqhjzlgl/202002/t20200223_765201.shtml (accessed May 8, 2021). (accessed May 21, 2021).
(51) National Development and Reform Commission. *Operation of Chinese Steel Industry from January to* February, 2020. https://www.ndrc.gov.cn/fgsj/tjsj/cyfz/zzyfz/202003/t20200331_1224736.html. (accessed May 8, 2021). (accessed May 8, 2021).
(52) Han, S.; Liu, J.; Hao, T.; Zhang, Y.; Li, P.; Yang, J.; Wang, Q.; Cai, Z.; Yao, Q.; Zhang, M.; Wang, X. Boundary layer structure and scavenging effect during a typical winter haze-fog episode in a core city of BTH region, China. *Atmos. Environ.* **2018**, *179*, 187−200.
(53) Zhang, Q.; Zheng, Y.; Tong, D.; Shao, M.; Wang, S.; Zhang, Y.; Xu, X.; Wang, J.; He, H.; Liu, W.; Ding, Y.; Lei, Y.; Li, J.; Wang, Z.; Zhang, X.; Wang, Y.; Cheng, J.; Liu, Y.; Shi, Q.; Yan, L.; Geng, G.; Hong, C.; Li, M.; Liu, F.; Zheng, B.; Cao, J.; Ding, A.; Gao, J.; Fu, Q.; Huo, J.; Liu, B.; Liu, Z.; Yang, F.; He, K.; Hao, J. Drivers of improved PM2.5 air quality in China from 2013 to 2017. *Proc. Natl. Acad. Sci. U. S. A.* **2019**, *116*, 24463−24469.

https://doi.org/10.1021/acs.est.1c05383
Environ. Sci. Technol. XXXX, XXX, XXX−XXX